iScience

CellPress

Article

Olfactory Object Recognition Based on Fine-Scale Stimulus Timing in *Drosophila*

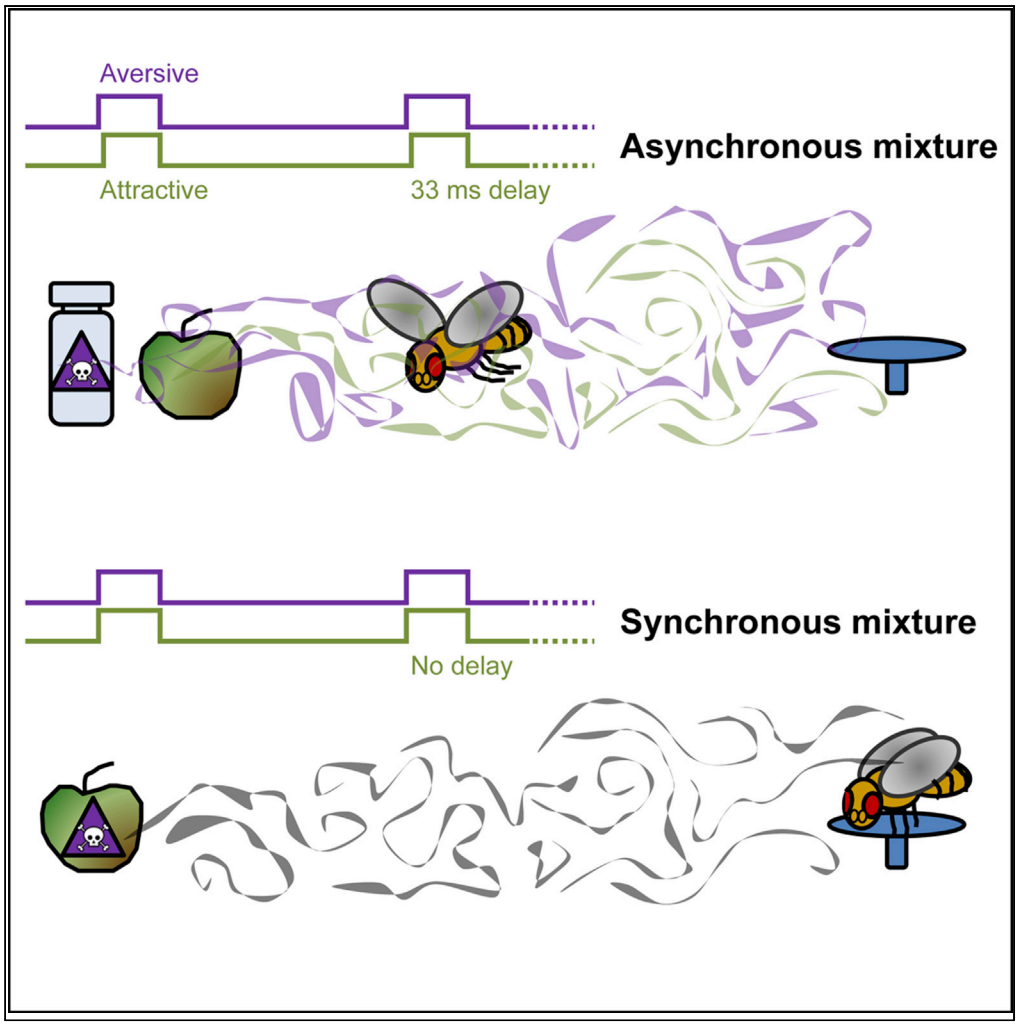

Aarti Sehdev, Yunusa G. Mohammed, Tilman Triphan, Paul Szyszka

paul@szyszkalab.com

HIGHLIGHTS

Flies can detect whether two mixed odorants arrive synchronously or asynchronously

This temporal sensitivity occurs for odorants with innate and learned valences

Flies' behavior suggests use of odor onset asynchrony for odor source segregation

Sehdev et al., iScience *13*, 113–124
March 29, 2019
https://doi.org/10.1016/j.isci.2019.02.014

iScience

CellPress

Article

Olfactory Object Recognition Based on Fine-Scale Stimulus Timing in *Drosophila*

Aarti Sehdev,[1,4] Yunusa G. Mohammed,[1,4] Tilman Triphan,[2] and Paul Szyszka[1,3,5,*]

SUMMARY

Odorants of behaviorally relevant objects (e.g., food sources) intermingle with those from other sources. Therefore to determine whether an odor source is good or bad—without actually visiting it—animals first need to segregate the odorants from different sources. To do so, animals could use temporal stimulus cues, because odorants from one source exhibit correlated fluctuations, whereas odorants from different sources are less correlated. However, the behaviorally relevant timescales of temporal stimulus cues for odor source segregation remain unclear. Using behavioral experiments with free-flying flies, we show that (1) odorant onset asynchrony increases flies' attraction to a mixture of two odorants with opposing innate or learned valence and (2) attraction does not increase when the attractive odorant arrives first. These data suggest that flies can use stimulus onset asynchrony for odor source segregation and imply temporally precise neural mechanisms for encoding odors and for segregating them into distinct objects.

INTRODUCTION

A natural scene is composed of simple stimuli, such as color, brightness, and movement of visual objects. In addition, it consists of relational stimuli that reflect the spatial and temporal correlations of those items that belong to the same object (e.g., the correlated movements of a person's body parts that allow us to segregate the person from the crowd). The mechanisms of how sensory systems use relational stimuli for object recognition are well understood in vision and audition. For example, humans use differences in stimulus onsets of a few tens of milliseconds to segregate visual objects from a background (Usher and Donnelly, 1998) or to segregate concurrent sounds from different sources (Hukin and Darwin, 1995). In contrast to vision and audition, olfaction research has mainly focused on simple stimuli, such as chemical identity, concentration, and dynamics of odorants (Galizia, 2014; Uchida et al., 2014), but it is largely unknown how the olfactory system processes relational stimuli that underlie olfactory object recognition.

Olfactory object recognition involves recognizing whether different odorants originate from the same or different sources (odor source segregation) (Hopfield, 1991). Odor source segregation can, in theory, be achieved from afar by analyzing the spatial distribution of odor plumes. The spatial distribution of odor plumes in the atmosphere is determined by the diffusion of odorant molecules and by the wind (Celani et al., 2014; Murlis et al., 2000). Because wind generally is turbulent, odor plumes are fragmented into filaments (similar to a plume of cigarette smoke). Because wind can transport odorant molecules much faster than diffusion, different odorants from the same source will largely stay together and will form a plume with relatively stable odorant concentration proportions (homogeneous plume). In contrast, odorants from different sources will be mixed by turbulent convection and will form a plume with variable odorant concentration proportions (heterogeneous plume).

Accordingly, plume heterogeneity enables animals to segregate odor sources (slugs [Hopfield and Gelperin, 1989], insects [Andersson et al., 2011; Baker et al., 1998; Saha et al., 2013; Szyszka et al., 2012], crabs [Weissburg et al., 2012]). But how do they do it? Animals could use temporal sampling for segregation, because in heterogeneous (multi-source) plumes the odorants from different sources exhibit less correlated fluctuations than in homogeneous (single-source) plumes (Celani et al., 2014; Hopfield, 1991). Thus, animals could use odorant onset asynchrony to detect that two odorants originate from different sources (Baker et al., 1998). Flying insects are particularly well adapted for detecting fine-scale temporal differences in odorant onset. Flying moths, for example, can segregate two odorants from two sources that are just 1 mm apart (Baker et al., 1998) and honey bees can use 6-ms short differences in odorant arrival

[1]University of Konstanz, Department of Biology, Neurobiology, Konstanz 78457, Germany

[2]University of Leipzig, Institute of Biology, Department of Genetics, Leipzig 04103, Germany

[3]Present address: University of Otago, Department of Zoology, Dunedin 9054, New Zealand

[4]These authors contributed equally

[5]Lead Contact

*Correspondence: paul@szyszkalab.com

https://doi.org/10.1016/j.isci.2019.02.014

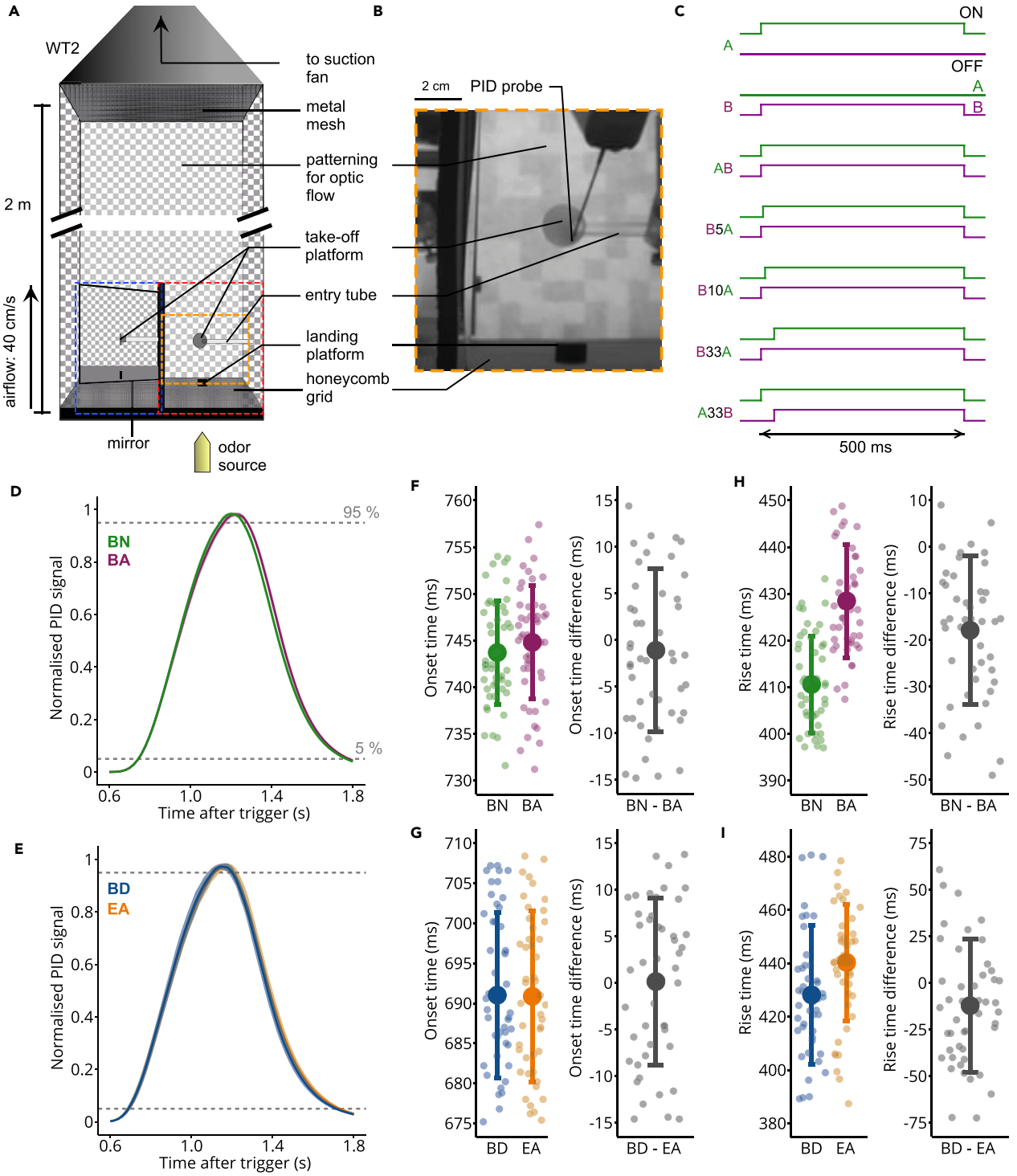

Figure 1. Delivering Temporally Precise Olfactory Stimuli in a Wind Tunnel

(A) Diagram of a wind tunnel 2 (WT 2). Red and blue dashed boxes indicate the captured x-y and z-y planes, respectively. The olfactory stimulator was placed outside the wind tunnel to minimize turbulences. The orange box outlines the image in (B).

(B) The layout of WT 2, showing the position where the odorant concentrations were recorded using a PID.

(C) Valve states for creating odorant pulses for the different stimuli. The attractive odorant A and aversive odorant B are represented in green and magenta, respectively. When asynchronous mixtures were presented, the first odorant was always given for 500 ms, and the following odorant with an onset delay. Both odorants had the same offset time. Pulses were repeated every 2 s.

Figure 1. *Continued*

(D) PID recordings of pulsed stimuli for the odorant pair with innate valence 2-butanone (BN, green) and butanal (BA, magenta) (mean and SD over 50 pulses). Valves opened for 500 ms. Each PID signal was normalized to the maximum concentration reached.

(E) Same as (D) for the odorant pair with conditioned valence 2,3-butanedione (BD, blue) and ethyl acetate (EA, orange), averaged over 50 pulses.

(F) Left: Onset time (time taken to reach 5% of maximum concentration after valve trigger) for BN and BA (mean and SD over 50 pulses). Individual points represent the onsets for each pulse. Right: Onset time difference between pairs of successive BN and BA pulses (mean and SD over 50 pulses).

(G) Same as (F) for BD and EA.

(H) Left: Rise time (time taken to reach 95% of maximum concentration from the 5% onset time) for BN and BA (mean and SD over 50 pulses). Individual points represent the rise times for each pulse. Right: Mean rise time difference between pairs of successive BN and BA pulses (mean and SD over 50 pulses).

(I) Same as (H) for BD and EA.

See also Figure S1.

for odor source segregation (Szyszka et al., 2012). Moreover, insects' rapid ligand-gated ionotropic olfactory receptors (Sato et al., 2008; Wicher et al., 2008) allow rapid and temporally precise odorant transduction (Egea-Weiss et al., 2018; Schuckel et al., 2008; Szyszka et al., 2014) and olfactory neurons are sensitive to stimulus onset asynchrony in the range of a few to tens of milliseconds (Broome et al., 2006; Meyer and Galizia, 2012; Nikonov and Leal, 2002; Saha et al., 2013; Stierle et al., 2013). However, the neural mechanisms of odor source segregation are still unknown.

Here we studied the capability of the fruit fly *Drosophila melanogaster* to use temporal stimulus cues for odor source segregation. We chose *Drosophila* because its genetic tractability will facilitate the determination of the causal relationship between behavioral odor source segregation and neural activity. We found that flies can detect a short difference in the arrival of two odorants (onset asynchrony of 33 ms). Odorant onset asynchrony increases flies' attraction to binary mixtures of odorants with opposing valence, suggesting that flies can use stimulus onset asynchrony for odor source segregation.

RESULTS

To test whether flies can use stimulus onset asynchrony for odor source segregation, we measured flies' attraction toward synchronous (to mimic one odor source) and asynchronous (to mimic two odor sources) binary mixtures of attractive and aversive odorants in a wind tunnel (Figure 1A). In each experimental trial a single fly walked into the wind tunnel through a tube, which ended on top of a take-off platform (Figure 1B). The air flow at the take-off platform had a speed of 40 cm/s. Odorant stimuli were applied with a custom-made stimulator (Raiser et al., 2016) that was located outside of the wind tunnel to prevent turbulences and to allow for temporally precise odorant stimuli. We tracked flies' flights in 3D and measured their odor attraction using odorants with either innate or conditioned valence (original data are available in Data S1). After each experimental trial we removed and discarded the fly.

The pairs of odorants with innate valence used were 2-butanone (BN) and butanal (BA) and BN and benzaldehyde (BZ). For the conditioned odorants, we used 2,3-butanedione (BD) and ethyl acetate (EA). We chose these odorants based on their innate valences measured in tethered flying flies (Badel et al., 2016), in which BN was attractive, whereas BA and BZ were aversive, and BD and EA were behaviorally neutral (note that in previous studies EA and BD were attractive in walking paradigms; Rodrigues and Siddiqi, 1978; Steck et al., 2012). To mimic homogeneous odorant plumes from one source we presented both odorants as a synchronous mixture (no onset delay between odorants). To mimic heterogeneous odorant plumes from different sources we presented both odorants as asynchronous mixtures (with 5- to 33-ms delays between odorant onsets) (Figure 1C). We used different wind tunnels (WT 1 and WT 2) and different arrangements of the landing platforms in an attempt to optimize experimental conditions (see Transparent Methods). However, we found no clear differences in flies' performance, indicating that the results are robust and do not depend on specific arrangements of the wind tunnels. To eliminate between-session variability, all data shown in a given panel of a figure were collected during the same experimental sessions. Accordingly, data points should be compared within panels, but not between panels.

Tracking of Temporally Well-Controlled Odorant Stimuli in the Wind Tunnel

We determined the temporal precision of stimulus delivery by measuring the stimulus dynamics with a photoionization detector (PID) (Figures 1D–1I and S1A–S1C). The inlet of the PID was placed at the surface of the take-off platform (Figure 1B). Each odorant was presented 50 times in three separate experimental sessions for the three odorant pairs BN/BA, BN/BZ, or BD/EA. The onset times

(time it took from valve opening to reach 5% of the maximum PID signal) were temporally precise across trials, with standard deviations ranging between 6 ms (BN, BA) and 10 ms (BD, EA) (Figures 1F, 1G, and S1B).

The onset times were similar for all odorant pairs (BN/BA, BN: 744 ± 6 ms, BA: 745 ± 6 ms; BN/BZ, BN: 750 ± 7 ms, BZ: 756 ± 7 ms; BD/EA, BD: 691 ± 10 ms, EA: 691 ± 10 ms; mean ± SD). The rise times (time it took to reach from 5% to 95% of the maximum PID signal) were also similar for the odorant pair BN/BA (BN, 411 ± 10 ms; BA, 428 ± 12 ms; mean ± SD) and for the odorant pair BD/EA (BD, 428 ms ± 26 ms; EA, 440 ms ± 21 ms), but less similar for the odorant pair BN/BZ (BN, 400 ± 12 ms; BZ, 444 ms ± 9 ms) (Figures 1H, 1I, and S1C). The differences in stimulus dynamics could be explained by the difference in the molecular mass between odorants, as stimulus dynamics gets slower with increasing molecular mass (in g/mol, BN, 72; BA, 72; BD, 86; EA, 88; BZ, 106) (Martelli et al., 2013; Raiser et al., 2016). Note, that part of the stimulus onset variability reflects the variability of the PID measurement itself and the actual stimulus dynamics may be less variable.

To visualize how flies explored space based on the odorant experience, we projected their flight trajectories on a plane and calculated the probability across flies to visit a particular pixel (visit probability, Figure 2A). When presented with the innately attractive odorant BN, flies were more likely to fly toward the target (which was either the actual odor source or a black platform near the odor source, see Transparent Methods) compared with the innately aversive odorant BZ. To assess the approach to the target, we counted the number of flies that reached halfway between the center of the take-off platform and the target (3.1 cm [117 pixels] for WT 1 and 2.7 cm [71 pixels] for WT 2) and calculated the approach probability by dividing this number by the total number of flies. Flies flew closer toward the target when stimulated with an attractive odorant than with an aversive odorant or a control air stimulus (Air) ($p(BN > BZ) > 0.999$ in Figure 2B; $p(BN > BA) = 0.962$, $p(BN > Air) > 0.999$ in Figure 2C; all statistical significances are given as Bayesian probabilities; see Transparent Methods and Table S2 for a comparison with frequentist statistics). However, in contrast to previous studies (van Breugel et al., 2018; Budick and Dickinson, 2006; Houot et al., 2017; Saxena et al., 2018), flies rarely landed at or near the target. This discrepancy might reflect the fact that, in contrast to these previous studies, our odorant delivery device was outside the wind tunnel. Positioning the odor delivery device inside the wind tunnel creates turbulences, and these turbulences could possibly provide localization cues for the fly to land. In contrast, our wind tunnel setting might mimic an odor source at a distance.

The percentage of flies that started flying ranged between 85% and 96% for the attractive odorant BN, ranged from 68% to 84% for the aversive odorants BZ or BA, and was 71% for the blank air control (Table S1). The average latency to flight ranged from 10–27 s, corresponding to 5–13 odorant pulses before taking off (Table S1, Figures S1H, S1J, S2D, and S2E). There was no consistent connection between the valence of an odorant and the latency to flight (e.g., latency to flight was longer for BZ than for BN (Figure S1H), but there was no difference for BN and BA (Figure S1J).

Attraction toward Asynchronous Mixtures of Odorants with Differing Innate Valence

To test whether flies can detect stimulus onset asynchrony, we presented the attractive odorant BN (A) and the aversive odorant BA (B) either as single odorants combined in a synchronous mixture (AB) or in asynchronous mixtures in which B preceded A by 33 ms (B33A) (Figure 3A). Note that we used the odorant pair BN/BA to test the effect of stimulus onset asynchrony rather than BN/BZ because the differences in stimulus dynamics between BN and BZ make this odorant pair unsuitable for generating synchronous mixtures (Figure S1).

Flies showed a higher approach probability for A compared with B ($p(A > B) = 0.998$) or with the synchronous mixture AB ($p(A > AB) = 0.993$) (Figure 3A). Moreover, flies showed a higher approach probability for the asynchronous mixture B33A compared with synchronous mixture AB ($p(B33A > AB) = 0.996$) or with the aversive odorant B ($p(B33A > B) > 0.999$). This shows that flies perceive the synchronous mixture AB and the asynchronous mixture B33A differently, with the onset asynchrony making the mixture more attractive.

To test whether flies are sensitive for shorter onset asynchronies we applied synchronous and asynchronous mixtures that started with B and with onset times differing by 5, 10, or 33 ms (B5A, B10A, B33A) (Figure 3B).

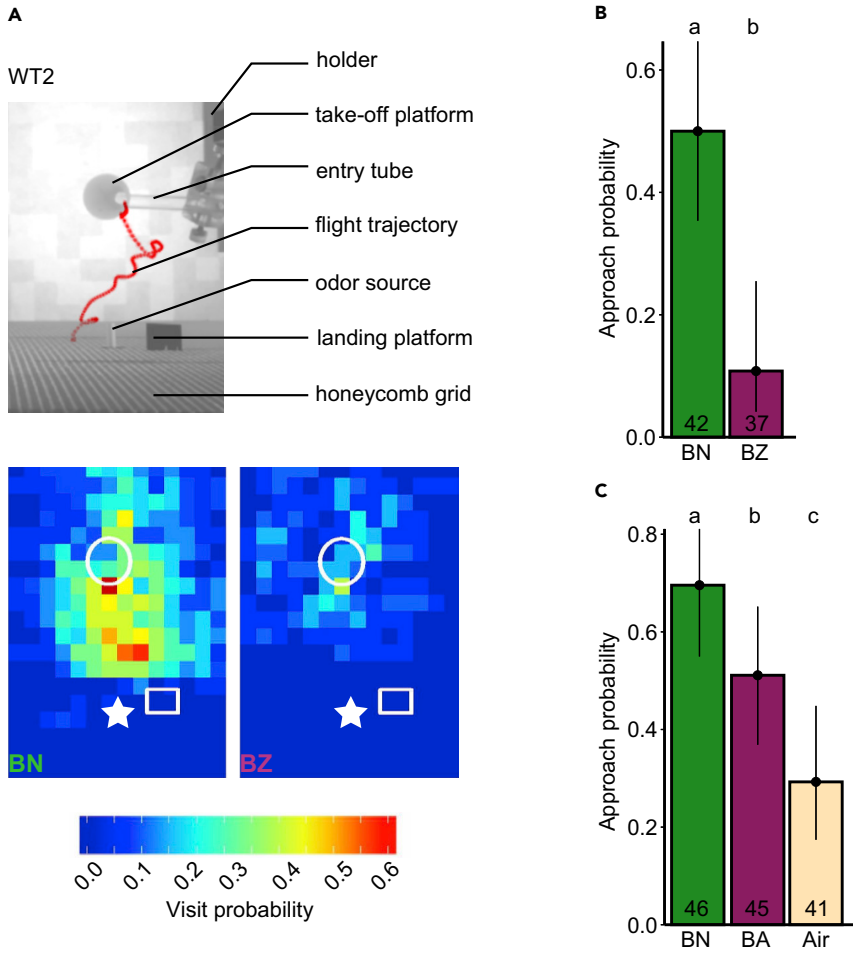

Figure 2. Odor Tracking in the Wind Tunnel

(A) Top: Flight trajectory of a flying fly (red) in the wind tunnel during stimulation with BN. Bottom: Visit probability map equivalent to top image for BN and BZ (set 1). Each bin represents 20 × 20 pixels in the image, corresponding to 7.6 × 7.6 mm at the height of the landing platform. Each bin shows the mean binary value across flies. The take-off platform (white circle), landing platform (white rectangle), and odor source (white star) are indicated for position reference. n = 24 and 20 for BN and BZ, respectively.

(B) Approach probability to cross the half distance between take-off platform and landing platform for BN and BZ. Bars represent the mean. Vertical lines represent the 95% credible intervals. The lower-case letters represent significantly different responses for the different odorants; this applies for all figures. Numbers in bars indicate the number of flies; this applies for all figures.

(C) Same as in (B) but for BN, butanal (BA), and a blank air stimulus (Air).

See also Figures S1 and S2.

Flies presented with A showed more activity in general, along with a higher visit probability near the target compared with flies presented with B. Flies showed a similar visit probability map for the synchronous mixture AB as for B. However, when stimulated with the asynchronous mixtures B33A, flies showed more activity near the target compared with AB and B.

To make the quantification of flies' approach behavior less arbitrary and to account for the fact that flies distributed differently in the two different wind tunnels and experimental sets, we calculated an approach area that segregated flies' approach probabilities for the attractive odorant A and the aversive odorant B the most (Figures 3C and S1–S3). We determined this area for each experimental set separately (see Transparent Methods). Note that this method maximizes the differences in approach probability between odorants A and B by design. Therefore we refrain from comparing flies' approach probabilities for A or B and restrict the comparisons to the mixtures.

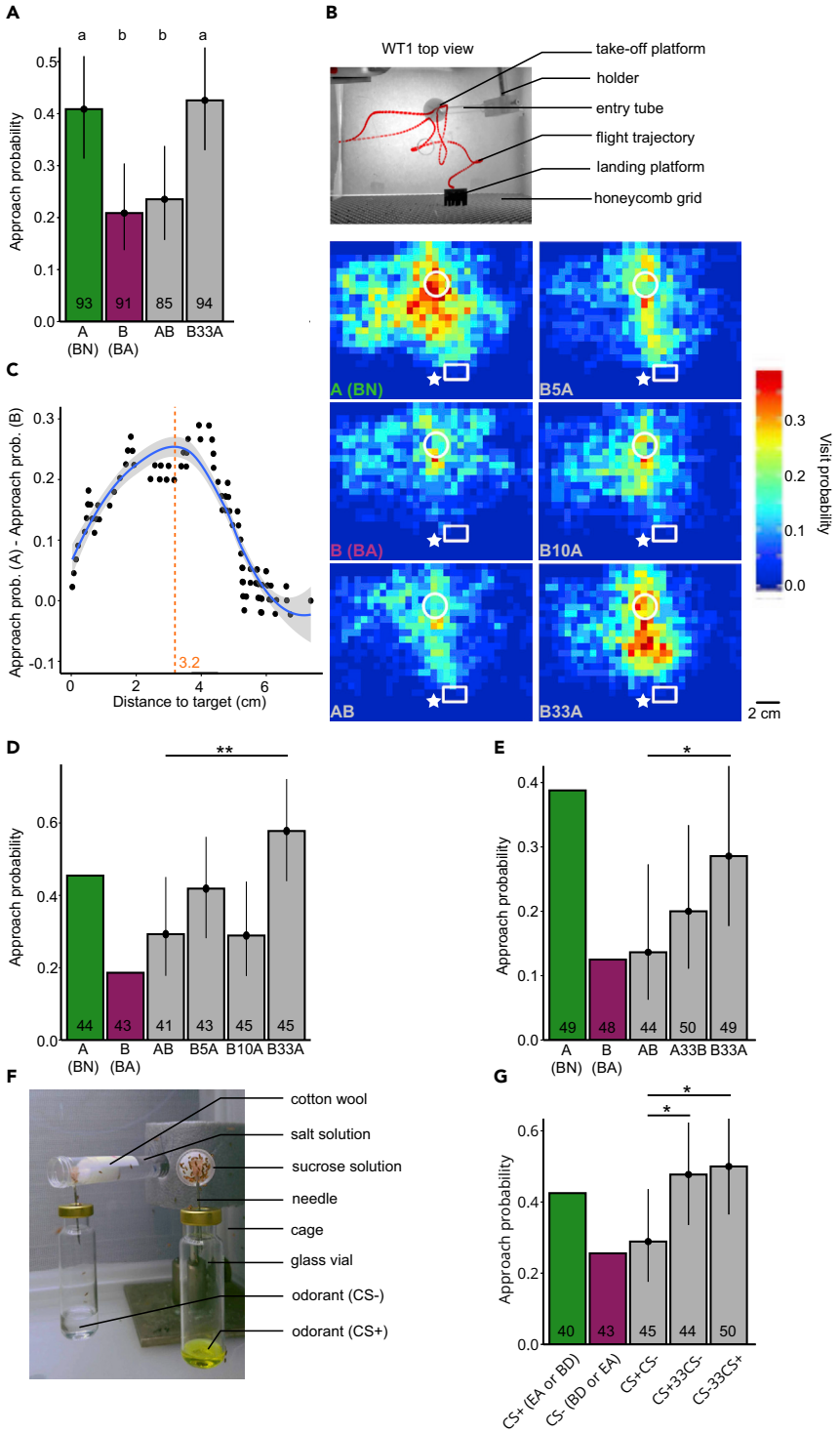

Figure 3. Stimulus Onset Asynchrony Makes a Mixture of Odorants with Differing Valences More Attractive

(A) Approach probabilities (determined by the half distance threshold) for the single odorants BN (A), BA (B), their synchronous mixture (AB), and their asynchronous mixture (B33A). Bars represent the mean. Vertical lines represent the 95% credible intervals. The lower-case letters represent significantly different responses to the odorant treatments (this dataset is pooled from experiments shown in D and E).

(B) Top: Flight trajectory of a flying fly (red) in the wind tunnel during stimulation with BN (A). Bottom: Visit probability maps for A (BN) and B (BA) and the synchronous (AB) and asynchronous (B5A, B10A, B33A) mixtures. The take-off platform

Figure 3. *Continued*
(white circle), landing platform (white rectangle), and odor source (white star) are indicated for position reference. n = 44, 43, 41, 43, 45, and 45 for A, B, AB, B5A, B10A and B33A, respectively.
(C) Thresholding method that uses the distance that separates flies' approach probabilities for A and B best (maximized A-B difference threshold). Each point represents the proportion of A-stimulated flies that approached the target by the given minimum distance to the target minus the proportion of B-stimulated flies. The blue trend line was fitted using locally weighted scatterplot smoothing. The gray area indicates the 95% confidence interval. The distance at the peak of the trend line was defined as threshold (orange dashed line and value).
(D) Approach probabilities (determined by the maximized A-B difference thresholding method) of the experiment to test flies' limit to detect onset asynchrony. Stars represent significantly different responses between AB and the other mixtures. As A and B are used to determine the threshold, they were not included in the statistical analysis.
(E) Approach probabilities (maximized A-B difference thresholding method) of the experiment to test the effect of odorant order in asynchronous mixtures.
(F) Conditioning setup in which flies were left for autonomous differential conditioning. Flies can freely fly in the cage and enter the odorized tubes containing cotton wool soaked either with aversive salt solution or attractive sucrose solution.
(G) Approach probability for odorant mixtures with conditioned valences (maximized A-B difference thresholding). Odorants BD and EA were used equally as often as the CS+ and CS−.
See also Figures S2 and S3.

The flies' responses to the mixtures depended on the timing between B and A (Figure 3D). For an onset asynchrony of 33 ms (B33A), flies were attracted to the target and scored a higher approach probability than for the synchronous mixture AB ($p(B33A > AB)$ = 0.995), similar to that of A alone. However, for onset asynchronies of 5 or 10 ms (B10A), flies' approach probabilities were not different from the approach probability for AB ($p(B5A > AB)$ = 0.894, $p(B10A > AB)$ = 0.500).

Next, we wanted to discern whether the order in which odorants are presented in a mixture affects how a fly perceives the mixture. We used the same paradigm and odorants as before and stimulated flies with the synchronous mixture AB and the asynchronous mixtures A33B (A precedes B) and B33A (B precedes A) (Figures 3E and S2). In this paradigm, flies showed a lower approach probability to the synchronous mixture AB than to the asynchronous mixture B33A ($p(B33A > AB)$ = 0.957)), confirming our previous result that B33A is perceived differently to AB, and is perceived by the fly as more attractive. However, the approach probability for the asynchronous mixture A33B was not significantly different from the approach probability for AB ($p(A33B > AB)$ = 0.793)).

These data show that flies can discriminate between the synchronous mixture AB and asynchronous mixture B33A, supporting the hypothesis that flies can use stimulus onset asynchrony to segregate the attractive component A from the mixture of A and B even if they never encountered A alone (in B33A, B started before A and A ended at the same time as B).

Attraction toward Asynchronous Mixtures of Odorants with Differing Learned Valence

Finally, we wanted to determine whether flies' capability to discriminate between synchronous and asynchronous mixtures only works for odorants with differing innate valence, or whether it also works for odorants with differing learned valences. To address this question, we used an autonomous differential conditioning paradigm and paired one odorant (positively conditioned stimulus, CS+) with a 1 M sucrose solution and another odorant (negatively conditioned stimulus, CS−) with a saturated NaCl solution (Figure 3F). We used the odorants EA and BD equally often for CS+ and CS−. Thus CS+ and CS− only differ with regard to the learned valences, devoid of odorant-specific innate valences.

Also in this experiment, flies discriminated between synchronous and asynchronous mixtures and showed lower approach probabilities to the synchronous mixture of CS+ and CS− (CS+CS−) than to the asynchronous mixture CS+33CS− or CS−33CS+ ($p(CS+33CS− > CS+CS−)$ = 0.965, $p(CS−33CS+ > CS+CS−)$ = 0.981) (Figures 3G and S3). Together, these findings support the hypothesis that flies can use stimulus onset asynchrony to segregate odorants with both learned and innate valences from mixtures.

DISCUSSION

We asked whether *Drosophila* can use stimulus onset asynchrony to segregate an attractive target odorant from a mixture with an aversive odorant. We found that flies show stronger attraction to asynchronous mixtures (mimicking two odorant sources) than to synchronous mixtures (mimicking one source). These results

suggest that the fly's olfactory system can use temporal stimulus cues for olfactory object recognition and odor source segregation.

Stimulus Cues for Odor Source Segregation

Insects, crabs, and slugs can segregate an attractive target odorant from an aversive odorant depending on whether both odorants originate from the same source (forming a homogeneous plume) or from different sources (forming a heterogeneous plume) (Andersson et al., 2011; Baker et al., 1998; Hopfield and Gelperin, 1989; Weissburg et al., 2012). To segregate two odorants from different sources, animals could in theory (1) use temporal sampling to detect time differences in odorant arrival, (2) use spatial sampling to detect the spatial heterogeneity of odorant concentrations along or between olfactory organs, or (3) recognize the target odorant during bouts of its pure, unmixed presence.

Our data suggest that flies can segregate a target odorant from an asynchronous mixture without ever encountering the target odorant in its unmixed form (in BΔtA, the target odorant A is always mixed with B, because A starts after and ends with B) and that odor source segregation is no better when the target odorant A arrives first. Therefore, in our experiments flies must have used spatial or temporal sampling for odor source segregation. Theoretically, flies could have used spatial sampling if they orient non-parallel to the wind direction. Then, in the case of an asynchronous mixture BΔtA, the downwind antenna could encounter odorant B, whereas the upwind antenna already encounters the mixture AB. However, this spatial difference in odorant input across both antennae will last for 1 ms at most, given that both antennae span around 0.4 mm and that the odorant stimulus moves at 40 cm/s. Thus the spatial cue across antennae has a much shorter duration (1 ms at most) than the temporal cue provided by the stimulus (33 ms). It is therefore likely that flies used temporal sampling for detecting the odorant onset asynchrony. The capability to segregate odor sources based on odorant onset asynchrony could allow flies to ignore bad objects (e.g., a spoiled food source where food and detrimental odorants originate from the same source) and to find a good object in a patch of bad objects (e.g., food and detrimental odorants originate from different sources) without actually visiting the source.

The odor source segregation paradigms that previous studies and our study used were odor recognition tasks in which the target odor either had an innate (Andersson et al., 2011; Baker et al., 1998; Weissburg et al., 2012) or a learned valence (Hopfield and Gelperin, 1989; Saha et al., 2013; Szyszka et al., 2012). Therefore the neural process of odor source segregation could occur during the encoding of odor identity or during the encoding of innate or learned odor valence. The small necessary odorant onset asynchrony for odor source segregation (33 ms in our study) poses temporal constraints on the precision of the neural code for odorant identity or valence, which we will discuss next.

Temporal Precision of the Neural Code for Odorant Identity

The temporal precision with which odorant identity can be encoded is limited by the temporal precision of stimulus-evoked action potentials (spikes) (Jeanne and Wilson, 2015). In *Drosophila*, the temporal precision of olfactory receptor neurons is high and the timing of the first odor-evoked spikes jitters with a standard deviation of down to 0.2 ms (Egea-Weiss et al., 2018). Olfactory receptor neurons of a given type (neurons that express the same olfactory receptor) coalesce in distinct glomeruli of the antennal lobe where they converge onto projection neurons. Compared with olfactory receptor neurons, projection neuron responses show less trial-to-trial variability and faster dynamics (Bhandawat et al., 2007). The high temporal precision and high spike rates of odor-evoked responses in *Drosophila* olfactory receptor neurons (de Bruyne et al., 1999; Egea-Weiss et al., 2018; Martelli et al., 2013) and projection neurons (Bhandawat et al., 2007; Wilson et al., 2004) would allow for rapid and temporally precise encoding of odorant identity. For example, odorant identity could be encoded within a few tens of milliseconds by reading out the increase in spike rates across the earliest responding neurons only (Krofczik et al., 2009; Nawrot, 2012), or by reading out the differences in response latencies across neurons (Brill et al., 2013; Egea-Weiss et al., 2018; Krofczik et al., 2009; Martelli et al., 2013; Müller et al., 2002; Paoli et al., 2018).

In *Drosophila*, there is evidence that the spike rates across the earliest responding neurons, and not the differences in response latencies, encode behaviorally relevant odorant identity information: downstream neurons in the mushroom body (Kenyon cells) are insensitive to response latency differences between projection neurons in the range of tens of milliseconds (Gruntman and Turner, 2013). We therefore propose that behaviorally relevant odorant identity information for odor source segregation is encoded in the spike

rates across the earliest responding projection neurons. This hypothesis is supported by the fact that downstream Kenyon cells generally have short integration time windows and respond to odorant onsets in a temporally precise manner (Demmer and Kloppenburg, 2009; Farkhooi et al., 2013; Ito et al., 2008; Perez-Orive, 2002; Szyszka et al., 2005; Turner et al., 2008).

Neural Responses to Synchronous and Asynchronous Odorant Mixtures

What is the neural correlate of odor source segregation based on odorant onset asynchrony? In the antennal lobe, synchronous odorant mixtures often induce neural activity patterns that lack part of the component information (synthetic mixture representation) (Deisig et al., 2006; Krofczik et al., 2009; Meyer and Galizia, 2012; Münch et al., 2013; Münch and Galizia, 2017; Silbering and Galizia, 2007). In contrast, asynchronous mixtures induce spatiotemporal activity patterns across projection neurons that partly match those evoked by the individual odorants (analytic mixture representation), and this asynchrony-induced shift from synthetic to more analytic mixture processing could support odor source segregation (Broome et al., 2006; Saha et al., 2013; Stierle et al., 2013) (for a modeling approach see Nowotny et al., 2013). However, the first arriving odorant often dominates the neural response to the asynchronous mixture, but such dominance of the first arriving odorant neither occurs in behavioral experiments in honey bees (Szyszka et al., 2012) nor in flies (this study). We therefore conclude that an asynchrony-induced shift from synthetic to a more analytic mixture representation in the antennal lobe cannot fully explain the behavioral odor source segregation observed in flies.

Alternatively, neural responses to both synchronous and asynchronous mixtures could contain sufficient analytical odorant information to allow for recognizing a target odorant. This hypothesis is supported by the observation that projection neurons that respond strongly to a single odorant generally also respond to its mixture with another odorant (Broome et al., 2006; Deisig et al., 2010; Saha et al., 2013; Silbering and Galizia, 2007; Stierle et al., 2013). Likewise, Kenyon cells that respond to a single odorant generally also respond to its mixture with another odorant (Campbell et al., 2013; Honegger et al., 2011; Shen et al., 2013). In addition, there is behavioral evidence for analytical processing of synchronous mixtures in *Drosophila*, as flies' responses to two odorants can add up linearly when presented as a synchronous mixture (Badel et al., 2016; Thoma et al., 2014). Moreover, flies fail in biconditional discrimination or negative patterning, tasks that require synthetic mixture processing (Young et al., 2011).

We therefore propose that (1) synchronous and asynchronous mixtures of odorants A and B activate a largely overlapping population of odorant-identity-encoding neurons (projection neurons and Kenyon cells), (2) this population includes both the A- and the B-activated neurons, and (3) odorant-identity-encoding neurons preserve the onset times of odorants A and B.

Neural Encoding of Odorant Valence and Odor Source Segregation

Stimulus-onset-asynchrony-induced timing difference between the A- and the B-activated projection neurons and Kenyon cells could be detected during the process of odorant recognition, i.e., during the transformation of the odorant identity code into a valence code. In insects, the innate odorant valence is encoded by lateral horn neurons (Jeanne et al., 2018; Jefferis et al., 2007; Roussel et al., 2014; Strutz et al., 2014), whereas learned odorant valence is encoded by mushroom body output neurons (Aso et al., 2014; Hige et al., 2015; Strube-Bloss et al., 2011). Both lateral horn neurons and mushroom body output neurons could preserve the temporal differences in odorant onsets: lateral horn neurons (in *Drosophila*) allow faster odorant detection than projection neurons (Jeanne and Wilson, 2015). Likewise, mushroom body output neurons (in honey bees) respond on average more rapidly to odorants than projection neurons (Strube-Bloss et al., 2012) and spike-timing-dependent plasticity (in locusts) enhances the synchronization of co-activated mushroom body output neurons (Cassenaer and Laurent, 2007).

Therefore, whether odorants A and B originate from one or two sources could be detected by coincidence-detecting neurons that receive input from valence-encoding lateral horn neurons or mushroom body output neurons. Those coincidence-detecting neurons would respond to synchronous input from the A- and B- activated valence-encoding neurons (A and B come from one source) but not to asynchronous input (A and B come from different sources). Coincidence detection could, for example, be mediated by N-methyl-D-aspartate (NMDA) glutamate receptors (Mayer et al., 1984). The existence of glutamatergic neurons and NMDA receptors in both the lateral horn and in the mushroom body (Sinakevitch et al.,

2010), and glutamatergic valence-encoding mushroom body output neurons in *Drosophila* (Aso et al., 2014; Owald et al., 2015), is consistent with this hypothetical mechanism.

Comparison with Mammalian Olfaction

Several studies have suggested that mammals have difficulties in segregating the single odorants from mixtures (e.g., Laing and Francis, 1989), but temporal differences in odorant arrival can help odor segregation: For example, in humans, stimulus onset asynchrony in tens of milliseconds impairs the detection of the following odorant (Laing et al., 1994) and in mice a delay in tens of seconds between a background odorant and a following target odorant facilitates the detection of the target odorant (Linster et al., 2007). However, it is currently unknown whether mammals can also use odorant onset asynchronies in millisecond range for odor source segregation. The timescales of olfactory processing in mice suggest that they could detect stimulus onset asynchrony in the tens of milliseconds range and use it for odor segregation: First, mice can identify odorants rapidly (within less than 200 ms) (Abraham et al., 2004; Uchida and Mainen, 2003). Second, odor-evoked spikes in olfactory bulb neurons can be temporally precise, with an average trial-to-trial standard deviation of just 12 ms (Shusterman et al., 2011). This high spike timing precision allows rapid odor coding, for example, by reading out the differences in response latencies (Haddad et al., 2013; Junek et al., 2010; Schaefer and Margrie, 2012; Spors, 2006) or by reading out the earliest responding neurons only (Wilson et al., 2017).

The next important steps will be to determine the behaviorally relevant stimulus timescales for odor source segregation in natural environments and to conduct causal studies on the underlying neural mechanisms. Doing this both in insects and mammals offers the possibility to reveal the differences and unifying principles of olfactory object recognition.

Limitations of the Study

The finding that flies show a higher approach to the asynchronous mixture B33A (the attractive odorant A arrives 33 ms after odorant B) than to the synchronous mixture AB shows that flies can detect stimulus onset asynchrony. However, it does not allow conclusions about the perceptual differences between B33A and AB. Thus we cannot discriminate between the proposed explanations that (1) flies perceive the attractive odorant A better in B33A than in AB or (2) flies perceive odorant A equally well in B33A and AB, and the 33-ms onset asynchrony adds the information that A and B originate from different sources. The question about the perceptual differences between AB and B33A could be answered to some extent by analyzing how neural responses to AB and B33A relate the responses of A and B alone.

METHODS

All methods can be found in the accompanying Transparent Methods supplemental file.

SUPPLEMENTAL INFORMATION

Supplemental Information can be found online at https://doi.org/10.1016/j.isci.2019.02.014.

ACKNOWLEDGMENTS

We thank Stefanie Neupert for advice on the statistics and comments on the manuscript, C. Giovanni Galiza, Thomas Nowotny, and Mario Pannunzi for comments on the manuscript and Cansu Tafrali for help with the experiments. This project was funded by the Human Frontier Science Program (RGP0053/2015 to PS.).

AUTHOR CONTRIBUTIONS

P.S. conceptualized and designed the study. Y.M.G. and A.S. performed the data collection. T.T. wrote the video processing script and provided expertise on the analysis. Y.G.M. and A.S. performed the video processing. A.S. performed the statistical analysis. P.S., Y.G.M., and A.S. wrote and edited the manuscript. P.S. supervised the study.

DECLARATION OF INTERESTS

The authors declare no competing interests.

Received: October 17, 2018
Revised: January 9, 2019
Accepted: February 12, 2019
Published: March 29, 2019

REFERENCES

Abraham, N.M., Spors, H., Carleton, A., Margrie, T.W., Kuner, T., and Schaefer, A.T. (2004). Maintaining accuracy at the expense of speed. Neuron *44*, 865–876.

Andersson, M.N., Binyameen, M., Sadek, M.M., and Schlyter, F. (2011). Attraction modulated by spacing of pheromone components and anti-attractants in a bark beetle and a moth. J. Chem. Ecol. *37*, 899–911.

Aso, Y., Sitaraman, D., Ichinose, T., Kaun, K.R., Vogt, K., Belliart-Guérin, G., Plaçais, P.Y., Robie, A.A., Yamagata, N., Schnaitmann, C., et al. (2014). Mushroom body output neurons encode valence and guide memory-based action selection in *Drosophila*. Elife *3*, e04580.

Badel, L., Ohta, K., Tsuchimoto, Y., and Kazama, H. (2016). Decoding of context-dependent olfactory behavior in *Drosophila*. Neuron *91*, 155–167.

Baker, T.C., Fadamiro, H.Y., and Cosse, A.A. (1998). Moth uses fine tuning for odour resolution. Nature *393*, 530.

Bhandawat, V., Olsen, S.R., Gouwens, N.W., Schlief, M.L., and Wilson, R.I. (2007). Sensory processing in the *Drosophila* antennal lobe increases reliability and separability of ensemble odor representations. Nat. Neurosci. *10*, 1474–1482.

van Breugel, F., Huda, A., and Dickinson, M.H. (2018). Distinct activity-gated pathways mediate attraction and aversion to CO2 in *Drosophila*. Nature *564*, 420–424.

Brill, M.F., Rosenbaum, T., Reus, I., Kleineidam, C.J., Nawrot, M.P., and Rossler, W. (2013). Parallel processing via a dual olfactory pathway in the honeybee. J. Neurosci. *33*, 2443–2456.

Broome, B.M., Jayaraman, V., and Laurent, G. (2006). Encoding and decoding of overlapping odor sequences. Neuron *51*, 467–482.

de Bruyne, M., Clyne, P.J., and Carlson, J.R. (1999). Odor coding in a model olfactory organ: the *Drosophila* maxillary palp. J. Neurosci. *19*, 4520–4532.

Budick, S.A., and Dickinson, M.H. (2006). Free-flight responses of *Drosophila melanogaster* to attractive odors. J. Exp. Biol. *209*, 3001–3017.

Campbell, R.A.A., Honegger, K.S., Qin, H., Li, W., Demir, E., and Turner, G.C. (2013). Imaging a population code for odor identity in the *Drosophila* mushroom body. J. Neurosci. *33*, 10568–10581.

Cassenaer, S., and Laurent, G. (2007). Hebbian STDP in mushroom bodies facilitates the synchronous flow of olfactory information in locusts. Nature *448*, 709–713.

Celani, A., Villermaux, E., and Vergassola, M. (2014). Odor landscapes in turbulent environments. Phys. Rev. X *4*, 1–17.

Deisig, N., Giurfa, M., Lachnit, H., and Sandoz, J.C. (2006). Neural representation of olfactory mixtures in the honeybee antennal lobe. Eur. J. Neurosci. *24*, 1161–1174.

Deisig, N., Giurfa, M., and Sandoz, J.C. (2010). Antennal lobe processing increases separability of odor mixture representations in the honeybee. J. Neurophysiol. *103*, 2185–2194.

Demmer, H., and Kloppenburg, P. (2009). Intrinsic membrane properties and inhibitory synaptic input of kenyon cells as mechanisms for sparse coding? J. Neurophysiol. *102*, 1538–1550.

Egea-Weiss, A., Renner, A., Kleineidam, C.J., and Szyszka, P. (2018). High precision of spike timing across olfactory receptor neurons allows rapid odor coding in *Drosophila*. IScience *4*, 76–83.

Farkhooi, F., Froese, A., Muller, E., Menzel, R., and Nawrot, M.P. (2013). Cellular adaptation facilitates sparse and reliable coding in sensory pathways. PLoS Comput. Biol. *9*, e1003251.

Galizia, C.G. (2014). Olfactory coding in the insect brain: data and conjectures. Eur. J. Neurosci. *39*, 1784–1795.

Gruntman, E., and Turner, G.C. (2013). Integration of the olfactory code across dendritic claws of single mushroom body neurons. Nat. Neurosci. *16*, 1821–1829.

Haddad, R., Lanjuin, A., Madisen, L., Zeng, H., Murthy, V.N., and Uchida, N. (2013). Olfactory cortical neurons read out a relative time code in the olfactory bulb. Nat. Neurosci. *16*, 949–957.

Hige, T., Aso, Y., Modi, M.N., Rubin, G.M., and Turner, G.C. (2015). Heterosynaptic plasticity underlies aversive olfactory learning in *Drosophila*. Neuron *88*, 985–998.

Honegger, K.S., Campbell, R.A.A., and Turner, G.C. (2011). Cellular-resolution population imaging reveals robust sparse coding in the *Drosophila* mushroom body. J. Neurosci. *31*, 11772–11785.

Hopfield, J.J. (1991). Olfactory computation and object perception. Proc. Natl. Acad. Sci. U S A *88*, 6462–6466.

Hopfield, J.F., and Gelperin, A. (1989). Differential conditioning to a compound stimulus and its components in the terrestrial mollusc Limax maximus. Behav. Neurosci. *103*, 329–333.

Houot, B., Gigot, V., Robichon, A., and Ferveur, J.-F. (2017). Free flight odor tracking in *Drosophila*: effect of wing chemosensors, sex and pheromonal gene regulation. Sci. Rep. *7*, 40221.

Hukin, R.W., and Darwin, C.J. (1995). Comparison of the effect of onset asynchrony on auditory grouping in pitch matching and vowel identification. Percept. Psychophys. *57*, 191–196.

Ito, I., Ong, R.C.-Y., Raman, B., and Stopfer, M. (2008). Sparse odor representation and olfactory learning. Nat. Neurosci. *11*, 1177–1184.

Jeanne, J.M., and Wilson, R.I. (2015). Convergence, divergence, and reconvergence in a feedforward network improves neural speed and accuracy. Neuron *88*, 1014–1026.

Jeanne, J.M., Fişek, M., and Wilson, R.I. (2018). The organization of projections from olfactory glomeruli onto higher-order neurons. Neuron *98*, 1198–1213.e6.

Jefferis, G.S.X.E., Potter, C.J., Chan, A.M., Marin, E.C., Rohlfing, T., Maurer, C.R., and Luo, L. (2007). Comprehensive maps of *Drosophila* higher olfactory centers: spatially segregated fruit and pheromone representation. Cell *128*, 1187–1203.

Junek, S., Kludt, E., Wolf, F., and Schild, D. (2010). Olfactory coding with patterns of response latencies. Neuron *67*, 872–884.

Krofczik, S., Menzel, R., and Nawrot, M.P. (2009). Rapid odor processing in the honeybee antennal lobe network. Front. Comput. Neurosci. *2*, 9.

Laing, D.G., and Francis, G.W. (1989). The capacity of humans to identify odors in mixtures. Physiol. Behav. *46*, 809–814.

Laing, D.G., Eddy, A., Francis, G.W., and Stephens, L. (1994). Evidence for the temporal processing of odor mixtures in humans. Brain Res. *651*, 317–328.

Linster, C., Henry, L., Kadohisa, M., and Wilson, D.A. (2007). Synaptic adaptation and odor-background segmentation. Neurobiol. Learn. Mem. *87*, 352–360.

Martelli, C., Carlson, J.R., and Emonet, T. (2013). Intensity invariant dynamics and odor-specific latencies in olfactory receptor neuron response. J. Neurosci. *33*, 6285–6297.

Mayer, M.L., Westbrook, G.L., and Guthrie, P.B. (1984). Voltage-dependent block by Mg2+of NMDA responses in spinal cord neurones. Nature *309*, 261–263.

Meyer, A., and Galizia, C.G. (2012). Elemental and configural olfactory coding by antennal lobe neurons of the honeybee (*Apis mellifera*). J. Comp. Physiol. A Neuroethol. Sens. Neural Behav. Physiol. *198*, 159–171.

Müller, D., Abel, R., Brandt, R., Zöckler, M., and Menzel, R. (2002). Differential parallel processing of olfactory information in the honeybee, *Apis mellifera L.* J. Comp. Physiol. A Neuroethol. Sens. Neural Behav. Physiol. *188*, 359–370.

Münch, D., and Galizia, C.G. (2017). Take time: odor coding capacity across sensory neurons increases over time in *Drosophila*. J. Comp. Physiol. A *203*, 959–972.

Münch, D., Schmeichel, B., Silbering, A.F., and Galizia, C.G. (2013). Weaker ligands can dominate an odor blend due to syntopic interactions. Chem. Senses *38*, 293–304.

Murlis, J., Willis, M.A., and Carde, R.T. (2000). Spatial and temporal structures of pheromone plumes in fields and forests. Physiol. Entomol. *25*, 211–222.

Nawrot, M.P. (2012). Dynamics of sensory processing in the dual olfactory pathway of the honeybee. Apidologie *43*, 269–291.

Nikonov, A.A., and Leal, W.S. (2002). Peripheral coding of sex pheromone and a behavioral antagonist in the Japanese beetle, *Popillia japonica*. J. Chem. Ecol. *28*, 1075–1089.

Nowotny, T., Stierle, J.S., Galizia, C.G., and Szyszka, P. (2013). Data-driven honeybee antennal lobe model suggests how stimulus-onset asynchrony can aid odour segregation. Brain Res. *1536*, 119–134.

Owald, D., Felsenberg, J., Talbot, C.B., Das, G., Perisse, E., Huetteroth, W., and Waddell, S. (2015). Activity of defined mushroom body output neurons underlies learned olfactory behavior in *Drosophila*. Neuron *86*, 417–427.

Paoli, M., Albi, A., Zanon, M., Zanini, D., Antolini, R., and Haase, A. (2018). Neuronal response latencies encode first odor identity information across subjects. J. Neurosci. *38*, 9240–9251.

Perez-Orive, J. (2002). Oscillations and sparsening of odor representations in the mushroom body. Science *297*, 359–365.

Raiser, G., Galizia, C.G.G., and Szyszka, P. (2016). A high-bandwidth dual-channel olfactory stimulator for studying temporal sensitivity of olfactory processing. Chem. Senses *42*, bjw114.

Rodrigues, V., and Siddiqi, O. (1978). Genetic analysis of chemosensory pathway. Proc. Indian Acad. Sci. Sect. B Exp. Biol. *87*, 147–160.

Roussel, E., Carcaud, J., Combe, M., Giurfa, M., and Sandoz, J.-C. (2014). Olfactory coding in the honeybee lateral horn. Curr. Biol. *24*, 561–567.

Saha, D., Leong, K., Li, C., Peterson, S., Siegel, G., and Raman, B. (2013). A spatiotemporal coding mechanism for background-invariant odor recognition. Nat. Neurosci. *16*, 1830–1839.

Sato, K., Pellegrino, M., Nakagawa, T., Nakagawa, T., Vosshall, L.B., and Touhara, K. (2008). Insect olfactory receptors are heteromeric ligand-gated ion channels. Nature *452*, 1002–1006.

Saxena, N., Natesan, D., and Sane, S.P. (2018). Odor source localization in complex visual environments by fruit flies. J. Exp. Biol. *221*, jeb172023.

Schaefer, A.T., and Margrie, T.W. (2012). Psychophysical properties of odor processing can be quantitatively described by relative action potential latency patterns in mitral and tufted cells. Front. Syst. Neurosci. *6*, 30.

Schuckel, J., Meisner, S., Torkkeli, P.H., and French, A.S. (2008). Dynamic properties of *Drosophila* olfactory electroantennograms. J. Comp. Physiol. A Neuroethol. Sens. Neural Behav. Physiol. *194*, 483–489.

Shen, K., Tootoonian, S., and Laurent, G. (2013). Encoding of mixtures in a simple olfactory system. Neuron *80*, 1246–1262.

Shusterman, R., Smear, M.C., Koulakov, A.A., and Rinberg, D. (2011). Precise olfactory responses tile the sniff cycle. Nat. Neurosci. *14*, 1039–1044.

Silbering, A.F., and Galizia, C.G. (2007). Processing of odor mixtures in the *Drosophila* antennal lobe reveals both global inhibition and glomerulus-specific interactions. J. Neurosci. *27*, 11966–11977.

Sinakevitch, I., Grau, Y., Strausfeld, N.J., and Birman, S. (2010). Dynamics of glutamatergic signaling in the mushroom body of young adult *Drosophila*. Neural Dev. *5*, 10.

Spors, H. (2006). Temporal dynamics and latency patterns of receptor neuron input to the olfactory bulb. J. Neurosci. *26*, 1247–1259.

Steck, K., Veit, D., Grandy, R., Badia, S.B.I., Badia, S.B.I., Mathews, Z., Verschure, P., Hansson, B.S., and Knaden, M. (2012). A high-throughput behavioral paradigm for *Drosophila* olfaction - the Flywalk. Sci. Rep. *2*, 361.

Stierle, J.S., Galizia, C.G., and Szyszka, P. (2013). Millisecond stimulus onset-asynchrony enhances information about components in an odor mixture. J. Neurosci. *33*, 6060–6069.

Strube-Bloss, M.F., Nawrot, M.P., and Menzel, R. (2011). Mushroom body output neurons encode odor – reward associations. J. Neurosci. *31*, 3129–3140.

Strube-Bloss, M.F., Herrera-Valdez, M.A., and Smith, B.H. (2012). Ensemble response in mushroom body output neurons of the honey bee outpaces spatiotemporal odor processing two synapses earlier in the antennal lobe. PLoS One *7*, e50322.

Strutz, A., Soelter, J., Baschwitz, A., Farhan, A., Grabe, V., Rybak, J., Knaden, M., Schmuker, M., Hansson, B.S., and Sachse, S. (2014). Decoding odor quality and intensity in the *Drosophila* brain. Elife *3*, e04147.

Szyszka, P., Ditzen, M., Galkin, A., Galizia, C.G.G., and Menzel, R. (2005). Sparsening and temporal sharpening of olfactory representations in the honeybee mushroom bodies. J. Neurophysiol. *94*, 3303–3313.

Szyszka, P., Stierle, J.S., Biergans, S., and Galizia, C.G. (2012). The speed of smell: odor-object segregation within milliseconds. PLoS One *7*, e36096.

Szyszka, P., Gerkin, R.C., Galizia, C.G.G., and Smith, B.H.B.H. (2014). High-speed odor transduction and pulse tracking by insect olfactory receptor neurons. Proc. Natl. Acad. Sci. U S A *111*, 16925–16930.

Thoma, M., Hansson, B.S., and Knaden, M. (2014). Compound valence is conserved in binary odor mixtures in *Drosophila melanogaster*. J. Exp. Biol. *217*, 3645–3655.

Turner, G.C., Bazhenov, M., and Laurent, G. (2008). Olfactory representations by *Drosophila* mushroom body neurons. J. Neurophysiol. *99*, 734–746.

Uchida, N., and Mainen, Z.F. (2003). Speed and accuracy of olfactory discrimination in the rat. Nat. Neurosci. *6*, 1224–1229.

Uchida, N., Poo, C., and Haddad, R. (2014). Coding and transformations in the olfactory system. Annu. Rev. Neurosci. *37*, 363–385.

Usher, M., and Donnelly, N. (1998). Visual synchrony affects binding and segmentation in perception. Nature *394*, 179–182.

Weissburg, M., Atkins, L., Berkenkamp, K., and Mankin, D. (2012). Dine or dash? Turbulence inhibits blue crab navigation in attractive-aversive odor plumes by altering signal structure encoded by the olfactory pathway. J. Exp. Biol. *215*, 4175–4182.

Wicher, D., Schäfer, R., Bauernfeind, R., Stensmyr, M.C., Heller, R., Heinemann, S.H., and Hansson, B.S. (2008). *Drosophila* odorant receptors are both ligand-gated and cyclic-nucleotide-activated cation channels. Nature *452*, 1007–1011.

Wilson, C.D., Serrano, G.O., Koulakov, A.A., and Rinberg, D. (2017). A primacy code for odor identity. Nat. Commun. *8*, 1477.

Wilson, R.I., Turner, G.C., and Laurent, G. (2004). Transformation of olfactory representations in the *Drosophila* antennal lobe. Science *303*, 366–370.

Young, J.M., Wessnitzer, J., Armstrong, J.D., and Webb, B. (2011). Elemental and non-elemental olfactory learning in *Drosophila*. Neurobiol. Learn. Mem. *96*, 339–352.

ISCI, Volume *13*

Supplemental Information

Olfactory Object Recognition Based on Fine-Scale Stimulus Timing in *Drosophila*

Aarti Sehdev, Yunusa G. Mohammed, Tilman Triphan, and Paul Szyszka

Supplemental Information

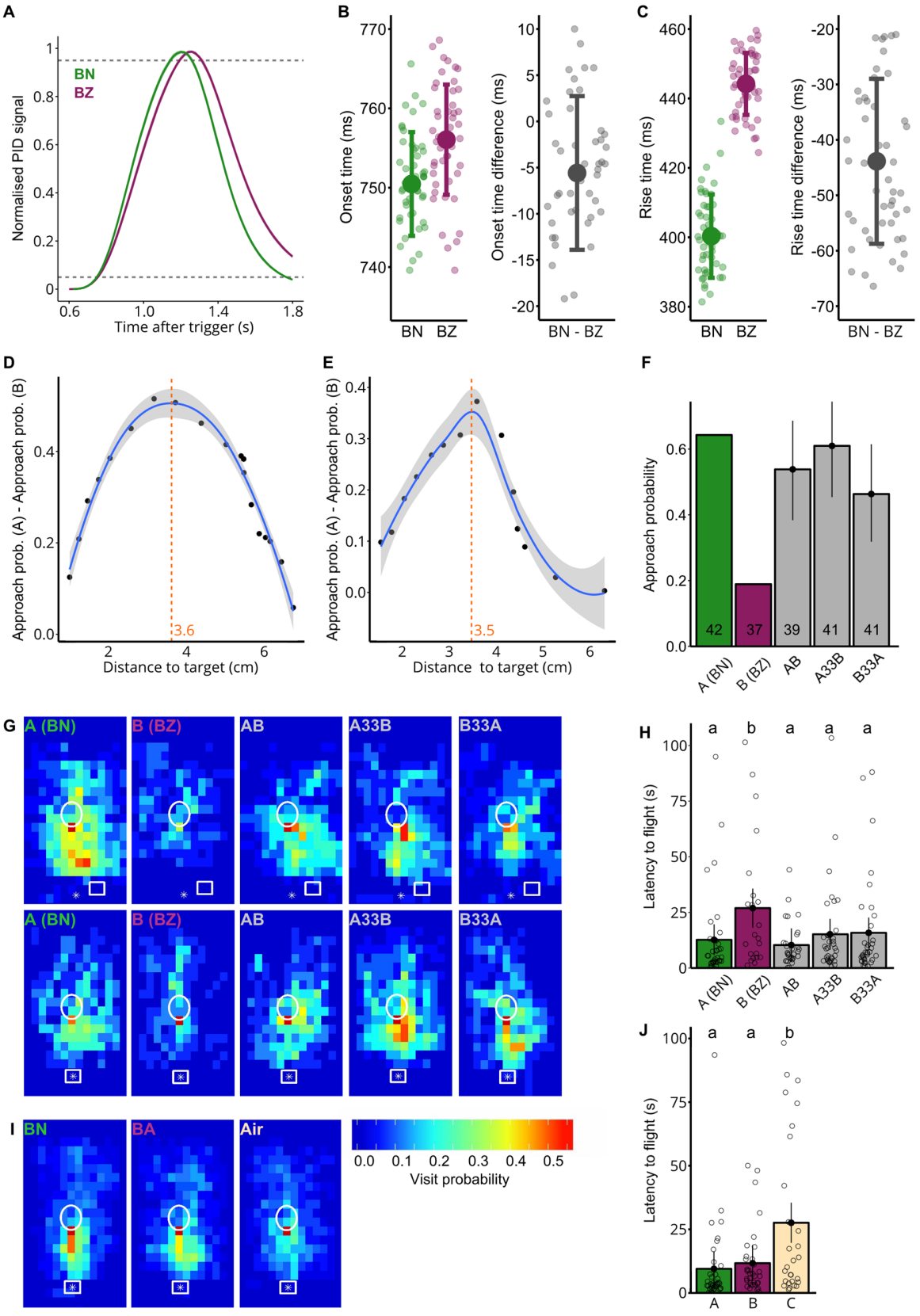

Figure S1. Stimulus timing and behavioral data, Related to Figure 1 and 2

(**A**) PID recordings of pulsed stimuli for the odorant pair with innate valence 2-butanone (BN, green) and benzaldehyde (BZ, magenta). Pulses were 500 ms long and with a 7 s interstimulus interval to allow the concentration to reach baseline again before the next pulse started (mean and SD over 50 pulses). Each PID signal was normalized to the maximum concentration reached. Grey dashed lines represent 5 and 95 % of the maximum.
(**B**) Left: Onset time (time taken to reach 5 % of maximum concentration after valve trigger) for BN and BZ (mean and SD over 50 pulses). Individual points represent the onsets for each pulse. Right: Onset time difference between pairs of BN and BZ pulses (mean and SD over 50 pulses).
(**C**) Left: Rise time (time take to reach 95 % of maximum concentration from the 5% onset time) for BN and BZ (mean and SD over 50 pulses). Individual points represent the rise times for each pulse. Right: Mean rise time difference between pairs of BN and BZ pulses (mean and SD over 50 Pulses).
(**D**) Thresholding method that uses the distance which separates flies' approach probabilities for (BN) A and (BZ) B best for set 1 (see "maximized A-B difference threshold" in Transparent Methods). Each point represents the proportion of A-stimulated flies that approached the target by the given minimum distance to the target minus the proportion of B-stimulated flies. The blue trend line was fitted using locally weighted scatterplot smoothing to avoid skewing by further away deviant points. The distance at the peak of the trend line was defined as threshold (orange dashed line and value)
(**E**) Same as (D) but for set 2 of BN and BZ.
(**F**) Approach probability for odorant mixtures with different asynchronies (maximized A-B difference threshold). Bars with vertical lines represent the mean and 95 % credible intervals. Since A and B are used to determine the threshold, they were not included in the statistical analysis.
(**G**) Visit probability maps of set 1 (Top) and set 2 (Bottom) of BN and BZ for single odorants and the mixtures. The take-off platform (white circle), landing platform (white rectangle) and odor source (white star) are indicated for position reference. n of set 1 = 24, 20, 22, 20 and 22; n of set 2 = 18, 17, 17, 21 and 19 for A, B, AB, A33B and B33A respectively.
(**H**) Response latency for odorants and mixtures, measured as the time taken from the fly entering the take-off platform to first flight. The lower case letters represent significantly different responses to the odorant treatments. Y axis limited to 110 s. n = 36, 25, 31, 37 and 37 for A, B, AB, A33B and B33A respectively.
(**I**) Same as (G) but for BN (A), BA (B) and blank air control (Air). n = 46, 45 and 41 for A, B, and C respectively.
(**J**) Same as (H) but for BN (A), BA (B) and blank air control (Air). n = 39, 34 and 29 for A, B and C respectively.

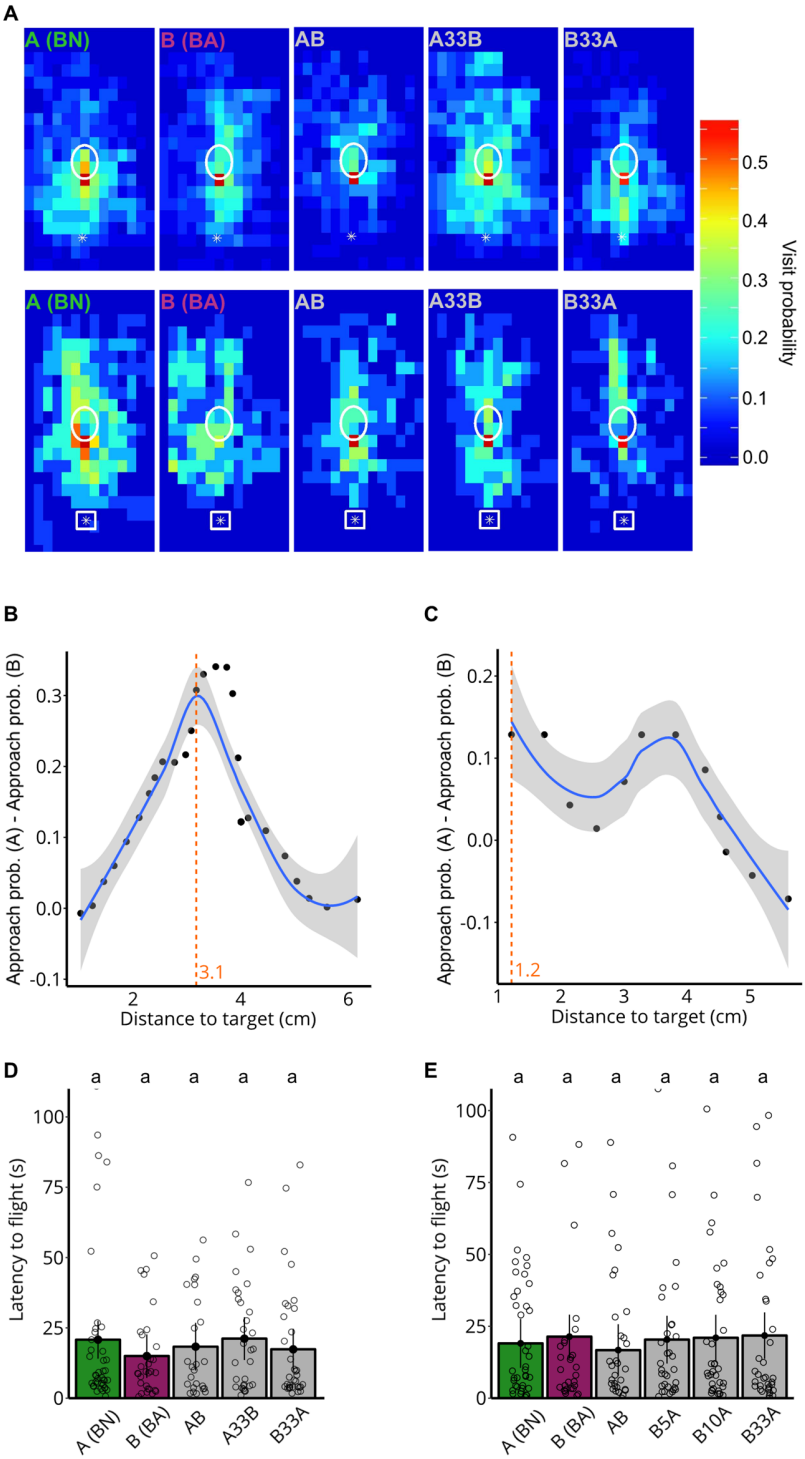

Figure S2. Behavioral data, Related to Figure 3B – E

(**A**) Visit probability maps of set 1 (Top) and set 2 (Bottom) of BN and BA for single odorants and the mixtures. The take-off platform (white circle), landing platform (white rectangle) and odor source (white star) are indicated for position reference. n for set 1 = 35, 34, 32, 35 and 33; n for set 2 = 14, 14, 12, 15 and 16 for A, B, AB, A33B and B33A respectively.

(**B**) Thresholding method that uses the distance which separates flies' approach probabilities for A and B best for set 1 of BN (A) and BA (B) (maximized A-B difference threshold).

(**C**) Same as (B) but for set 2 of BN and BA.

(**D**) Response latency for odorants and mixtures, measured as the time taken from the fly entering the take-off platform to first flight for the experiment shown in Figure 3E. The lower case letters represent significantly different responses to the odorant treatment. Y axis limited to 110 s. n = 42, 33, 28, 36 and 34 for A, B, AB, A33B and B33A respectively.

(**E**) Same as in (D) but for the experiment shown in Figure 3D. n = 42, 36, 33, 38, 36 and 39 for A, B, AB, B5A, B10A and B33A respectively.

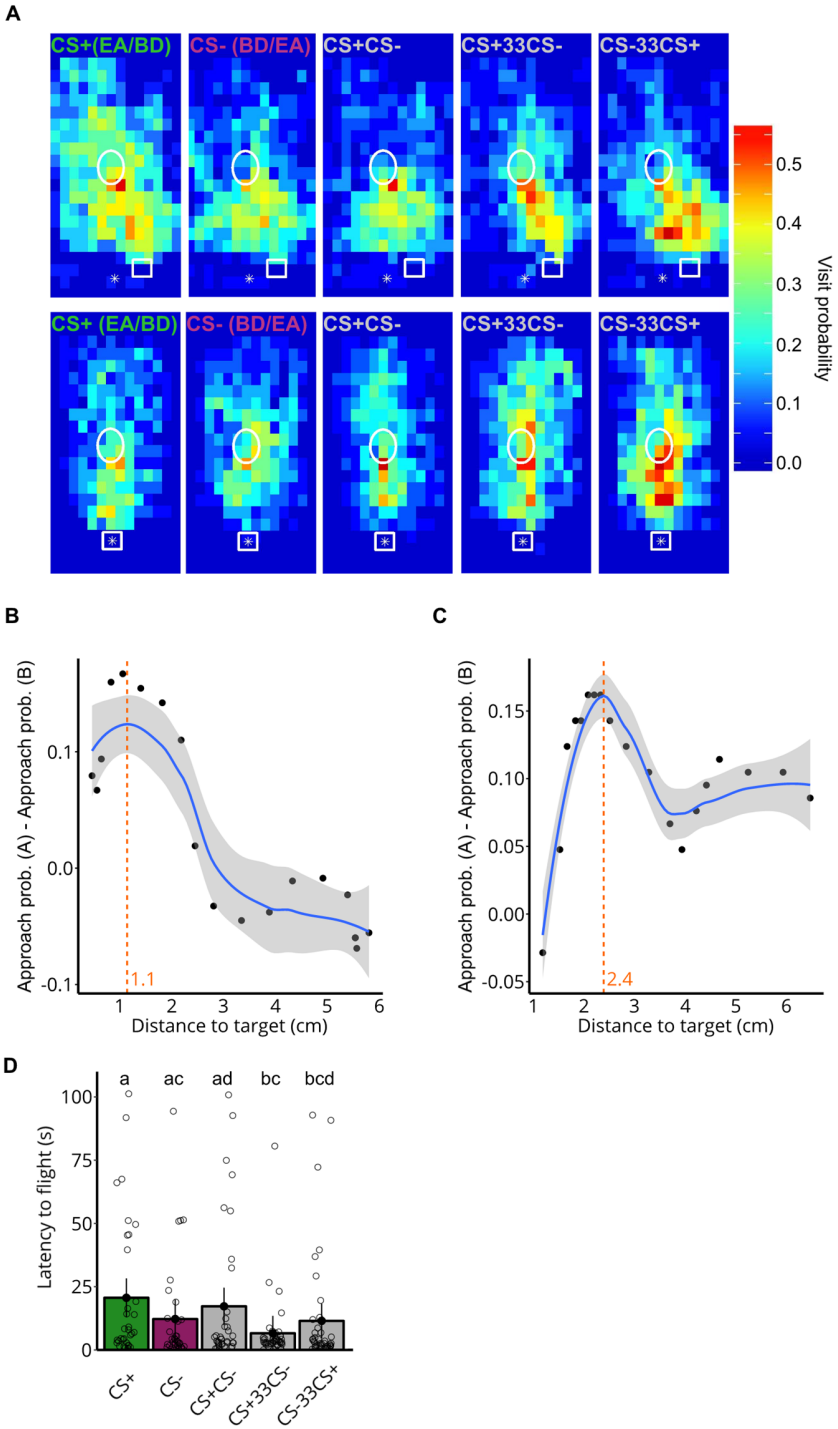

Figure S3. Behavioral data, Related to Figure 3G

(**A**) Visit probability maps of set 1 (Top) and set 2 (Bottom) of CS+ and CS- (either EA or BD) for single odorants and the mixtures. The take-off platform (white circle), landing platform (white rectangle) and odor source (white star) are indicated for position reference. n for set 1 = 19, 22, 23, 24 and 26; n for set 2 = 21, 21, 22, 20 and 24 for CS+, CS-, CS+CS-, CS+33CS- and CS-33CS+ respectively.

(**B**) Thresholding method that uses the distance which separates flies' approach probabilities for CS+ and CS- best for set 1 of EA and BD (maximized A-B difference threshold)

(**C**) Same as (B) but for set 2 of EA and BD.

(**D**) Response latency for odorants and mixtures, measured as the time taken from the fly entering the take-off platform to first flight. The lower case letters represent significantly different responses to the odorant treatments. Y axis limited to 110 s. n = 35, 37, 38, 43 and 46 for CS+, CS-, CS+CS-, CS+33CS- and CS-33CS+ respectively.

Table S1. Percentage of flies flying and their latency to flight, Related to Figure 2 and 3

Experiment	Stimulus	Total number of flies tested	Percentage of flies flying	Mean latency to flight (s)
Figure 2B, Figure S1D-H	A (BN)	42	86	13
	B (BZ)	37	68	27
	AB	39	80	10
	A33B	41	90	15
	B33A	41	90	16
Figure 2C	A (BN)	46	85	10
	B (BA)	45	76	12
	Air	41	71	28
Figure 3A	A (BN)	93	90	21
	B (BA)	91	76	16
	AB	85	72	19
	B33A	94	78	20
Figure 3D	A (BN)	44	96	19
	B (BA)	43	84	21
	AB	41	80	17
	B5A	43	88	20
	B10A	45	80	21
	B33A	45	87	22
Figure 3E, Figure S2	A (BN)	49	86	21
	B (BA)	48	70	15
	AB	44	64	18
	A33B	50	72	21
	B33A	49	70	17
Figure 3G, Figure S3	CS+ (EA/BD)	40	88	21
	CS- (BD/EA)	43	86	12
	CS+CS-	45	84	17
	CS+33CS-	44	92	7
	CS-33CS+	50	98	12

Table S2. Additional statistical analysis of approach probabilities using the exact binomial test, Related to Figure 2 and 3

P-values and corrected alpha values are given for the exact binomial test and Bayesian probabilities are given for the Bayesian analysis. Red values indicate significant differences.

Experiment	Odorants	Comparison	P-value	Corrected alpha	Bayesian probability
Figure 2B	BN (A), BZ (B)	A vs B	<0.001	0.05	>0.999
Figure 2C	BN (A), BA (B), Air	A vs B	<0.01	0.025	0.962
		A vs Air	<0.001	0.025	>0.999
Figure 3A	BN (A), BA (B)	A vs AB	<0.001	0.017	0.993
		B vs AB	0.62	0.017	0.338
		B33A vs AB	<0.001	0.017	0.996
Figure 3D	BN (A), BA (B)	B5A vs AB	0.1	0.017	0.894
		B10A vs AB	1.0	0.017	0.5
		B33A vs AB	<0.001	0.017	0.995
Figure 3E	BN (A), BA (B)	A33B vs AB	0.21	0.025	0.793
		B33A vs AB	<0.01	0.025	0.957
Figure 3G	EA/BD (CS+), BD/EA (CS-)	CS+33CS- vs CS+CS-	<0.05	0.025	0.965
		CS-33CS+ vs CS+CS-	<0.01	0.025	0.981

TRANSPARENT METHODS

Animals

Wild-type Canton S *Drosophila melanogaster* were reared on standard medium (100 mL contain 7.1 g cornmeal, 6.7 g fructose; 2.4 g dry yeast, 2.1 g sugar beet syrup, 0.7 g agar, 0.61 ml propionic acid, and 0.282 g ethyl paraben) under a 12:12 hours light:dark cycle (light from 09:00 to 21:00), at 25 °C and 60% relative humidity. All flies used in the experiments were female, aged between four and eight days old.

Wind tunnel

We carried out experiments in two wind tunnels, referred to here as wind tunnel 1 (WT 1, data shown in Figure 3D) and wind tunnel 2 (WT 2 data shown in all other figures). We filmed each experiment using Raspberry Pi cameras (Raspberry Pi Camera Module v2; Raspberry Pi 3 model B) for 2 or 3 minutes with a resolution of 640 x 480 pixels and 90 frames s^{-1}; the first 10 seconds of flight duration were used for the analysis.

Both wind tunnels were constructed from clear Plexiglas. The inner side walls and floor were covered by a random checker board pattern (grey on white paper). The dimension of WT 1 was 1.2 m x 0.19 m x 0.19 m and of WT 2 was 2 m x 0.40 m x 0.40 m. The exhaust took in room air (28 °C, 60 % relative humidity) through the tunnel and removed it from the setup building via a ventilation shaft. An aluminum honeycomb grid (hole diameter x length: 0.53 cm x 3 cm, WT 1; 0.32 cm x 9.7 cm, WT 2) at the inlet and a grid at the outlet of the tunnel created a non-turbulent flow throughout. The wind speed was 40 cm/s. We injected odorants into the inlet of the wind tunnel with an olfactory stimulator (Raiser et al., 2016). The outlet of the olfactory stimulator was 1 cm in diameter and was placed just outside of the honey comb grid, creating a non-turbulent air-stream within the tunnel that allowed us to control the timing of the odorant stimuli. Flies entered the tunnel through a glass tube that was connected to a take-off platform whose center was 7.5 cm (WT 1) or 6 cm (WT 2) downstream from the inner side of the honeycomb grid.

In the course of most of the experimental protocols (see below) we added a black landing platform at the honey comb grid near the entry site of the odorant plume. We introduced this landing platform in an attempt to increase flies approach behavior for attractive odorants, because recent studies have demonstrated that *Drosophila* approach dark spots when stimulated by an attractive odorant (Breugel et al., 2017; Saxena et al., 2018). Experimental protocols that differ with respect to the existence or position of a landing platform are referred to as “set 1”or “set 2” respectively. In WT 1 we used two cameras to film the flies. One camera was placed above the wind tunnel to capture the x-y plane of movement, whereas the other was placed at the side of the wind tunnel (90° to the other camera), thus capturing the movement of the fly within the z-y plane. The volume filmed measured 17.3 cm x 13.0 cm x 17.3 cm (x, y, z). In WT 2 we used a single camera placed above the wind tunnel to record the fly trajectories in the x-y plane. In order to capture the z-y plane of the flight track, we positioned a mirror at a 45° angle to the camera inside of the wind tunnel. The volume filmed measured 13.7 cm x 10.3 cm x 9.5 cm (x, y, z). Both wind tunnels were illuminated with indirect, homogeneous, white light with a color

temperature of 6500 K (WT 1: compact fluorescent light, tageslichtlampe24.de; WT 2: LEDs, led-konzept.de). Additionally, we used 850 nm backlight illumination (96 LED IR Lamp, Conrad; plus 2 cm thick polyethylene foam as diffusor) to get contrast-rich images of the flies.

Odorant delivery

Odorants were delivered into the wind tunnels using a custom-made multichannel olfactory stimulator (Raiser et al., 2016). All odorants were supplied by Sigma Aldrich. Pure odorants were stored in 20 ml glass vials (Schmidlin) sealed with a Teflon septum. The cross section of the odorant surface was 3.1 cm^2. The headspace of odorized air was permanently drawn into the air dilution system using flowmeters (112-02GL, Analyt-MTC) and an electronic pressure control (35898; Analyt-MTC). The stimulator had three channels: one for each odorant and one for blank air. The odorant vials were constantly flushed with clean air throughout the experiment, so that the headspace concentration reached a steady state of odorant evaporation into the air and odorant removal by the air flush. Note that due to the permanent air stream the headspace odorant concentration never saturated. The total flow per odorant channel was always 300 ml min^{-1}. In WT 1, BN was released at 50 ml min^{-1} and added to 250 ml min^{-1} air, and BA was released at 30 ml min^{-1} and added to 270 ml min^{-1} air (experiments in Figure 3). In WT 2, BN, BA and BZ were released at 50 ml min^{-1} and were added to 250 ml min^{-1} air (experiments in Figures 2 and 3). For the conditioned odorants we used the PID to determine the head space concentrations in the conditioning tubes (see below) by moving the PID needle rapidly into the conditioning tubes to prevent dilution in odorant concentration due to air suction of the PID. These concentrations from the conditioning paradigm were then adjusted in the odor delivery device by measuring the odorant concentration just above the take-off platform with the PID. EA was released at 4 ml min^{-1} and added to 296 ml min^{-1} air, and BD was released at 1.84 ml min^{-1} and added to 298.16 ml min^{-1} air (experiments in Figure 3).

The two odorant channels and a blank channel (each with an airstream of 300 ml min^{-1}) were combined and injected into a carrier air stream of 410 ml min^{-1} and, resulting in a total air flow at the outlet of the stimulator of 1.31 L min^{-1}, and a wind speed of 0.4 ms^{-1}.

Stimuli were presented either as single odorants (either A or B), as a synchronous mixture of odorants presented simultaneously (AB) or as an asynchronous mixture, with different time delays between the release of the odorants. In BΔtA, B starts before A, with Δt being either 5 ms, 10 ms or 33 ms. In AΔtB, A starts before B, with Δt being 33 ms (Figure 1C). Note that the trailing odorant ended at the same time as the preceding odorant. Stimuli were delivered in odorant pulses of 500 ms, and the interstimulus interval was 2 s. To exclude that differences in flies' approach behavior towards the asynchronous and synchronous mixture reflected responses to mechanical cues produced by valve switching, we applied the single odorants together with a 33 ms delayed blank stimulus (both stimuli ended at the same time).

During experiments, all odorants were removed from the wind tunnel via an exhaust into the outside atmosphere. Between experimental sessions using different odorants, the stimulator valves were flushed out over night to remove any residual odorants. Valves were controlled by compact RIO systems equipped with digital I/O modules Ni-9403 and odorant delivery was controlled by software written by Stefanie Neupert in LabVIEW 2011 SP1 (National Instruments).

Experimental protocol for odorants with innate valence

Day 1: Between 13:00 and 16:00, approximately 100 adult flies were removed from standard corn meal agar food and were subjected to food and water starvation for 24 hours in a cage (30×30×30 cm, BugDorm-1, BugDorm) that allowed them to move around freely, in a room with an approximate relative humidity of 60%, a temperature of 25 - 28 °C and 12 hour daylight cycle.

Day 2: Between 15:00 and 20:00, individual, flying female flies were removed from the cage and placed into a PVC tube through which they could walk freely to enter the wind tunnel and reach the take-off platform. For each experimental trial we used a single fly. Once the fly reached the take-off platform, odorant stimulation started. Each fly was stimulated repeatedly with the same odorant stimulus. After each experimental trial we removed and discarded the fly. During one experimental session (for a data set shown in a given panel of a figure), an equal number of flies were stimulated with the different stimuli so that between-session variability would affect the behavior to all stimuli equally. The order of stimuli was alternated.

Most of the experimental paradigms were made up of different sets, depending on the presence and location of the black landing platform. In the experiment shown in Figure 2A, 2B and S3, set 1 placed the landing platform 1.5 cm to the right of the odor source, whereas set 2 placed the platform at the odor source directly. In the experiment shown in Figure 2C, S1I and S1J, there was only one set, with the landing platform placed centrally at the location of the odor source. In the experiment shown in Figure 3B and 3D, there was only one set, where

the black platform was located 0.5 cm to the right of the odor source. For the experiments shown in Figure 3E, S2A-C, set 1 contained no landing platform, whereas set 2 contained the landing platform at the location of the odor source.

Differential conditioning

Day 1: Between 15:00 and 16:00, approximately 100 adult flies were removed from standard corn meal agar food and put into a cage (30×30×30 cm, BugDorm-1, BugDorm) that contained a differential conditioning apparatus (Figure 3F). Flies could move around freely at an approximate relative humidity of 30%, a temperature of 25 - 28 °C and normal 12 hour daylight cycle for 24 h.

We trained flies in a differential conditioning paradigm to associate one odorant (positively conditioned stimulus, CS+) with 1 M sucrose solution as the positive reinforcer and to associate another odorant (negatively conditioned stimulus, CS-) with saturated NaCl solution as negative reinforcer (Figure 3F). We used BD and EA as conditioned odorants. We balanced the experiments so that in half of the experiments we used BD as CS+ and EA as CS- and vice versa. CS+ and sucrose solution and CS- and NaCl solution were applied via two horizontally positioned plastic tubes (15 ml, 120 x 17 mm; Sarstedt). Each tube contained 10 ml of either sucrose or NaCl solution and were plugged with a cotton wool to avoid spillage. The frontal 2 cm of each tube remained empty. The odorant was delivered into this empty space via diffusion through a shortened head of a needle (1.2 x 40 mm, Sterican) which ended 1.5 cm inside the empty space of the tube. The needle was connected with a 20 ml glass vial (Schmidlin) that contained the pure odorant and was sealed with a Teflon septum. Thus, to reach the sucrose or NaCl solution, flies had to move through odorized air inside the plastic tube.

Day 2: Between 15:00 and 16:00, the conditioning apparatus was removed and flies were subjected to food and water starvation for the following 24 h in a room with an approximate relative humidity of 60%, a temperature of 25 - 28 °C and normal 12 hour daylight cycle.

Day 3: Flies were tested in the wind tunnel as described above in the section “Experimental protocol for odorants with innate valence” (Day 2).

The conditioning experiments (Figure 3G, S3) also had two sets, depending on the location of the black landing platform. In set 1, the black platform was located 1.5 cm to the right of the odor source, and in set 2, the black platform was at the location of the odor source.

Stimulus dynamics

To assess the dynamics and precision of the different stimuli, we used a photoionization detector (PID; miniPID model 200B; Aurora Scientific) to record the concentration change of pulses of each of the odorant pairs (BN and BA, BN and BZ, BD and EA) within the wind tunnel. Each pulse had a duration of 500 ms, and an interstimulus interval of 7 s to allow the odorant to clear from the odor delivery device and/or PID and to allow the PID signal to return to baseline before the following pulse was given. We gave a sequence of 100 pulses, alternating between odorant A and odorant B (7 s interval between A and B), thus 50 pulses of each odorant. For each odorant pulse, we calculated the onset time as the time it took to reach 5 % of the maximum PID signal, and the rise time as the time it took for the PID signal to reach from 5 % to 95 % of its maximum. We also calculated the difference in both the onset times and in the rise times between each of the 50 pairs of successive pulses (A – B) (we compared pairs of successive pulses to reduce the variability due to minor changes in wind speed in the wind tunnel which was affected by the wind speed outside).

Calculating flies’ distance to the target

To calculate the Euclidean distance to the source, we obtained the x, y and z coordinates of the fly for the first 10 s of flight of the recording. For the experiments shown in Fig. 3D, if a fly did not take off, we calculated its closest distance to the target. For all other experiments, if a fly did not take off we took the closest distance between the take-off platform and the target.

For WT 1, we used two cameras. Both cameras were triggered simultaneously with a TTL pulse, however to ensure that they did not go out of sync, all videos were aligned by first frame of flight. We calculated the Euclidean distance of the fly to the target:

Euclidean distance = $\sqrt{(x - x_0)^2 + (y - y_0)^2 + (z - z_0)^2}$

Where x, y and z are the coordinates of the fly’s location in a particular frame, and x0, y0 and z0 are the coordinates of the target.

For WT 2, a single camera was used to film the fly trajectories in the x and y plane. In order to record the movement in the z plane simultaneously, a mirror was placed at 45° to the x-y plane. Thus on the right half of the video recordings, the x-y plane was recorded, and on the left half of the video, the mirrored z-y plane was recorded. However, this resulted in the image in the left half shrinking to 1.3 times smaller than the original objects on the right half. Therefore, we calculated the fly’s distance to the target in WT 2 by:

Euclidean distance = $\sqrt{(x - x_0)^2 + (y - y_0)^2 + ((z - z_0) * 1.3)^2}$

Where x, y and z are the coordinates of the fly's location in a particular frame, and x0, y0 and z0 are the coordinates of the target

Quantifying flies' approach with the "half-distance threshold"

In order to measure approach behavior, we used the halfway distance between the frontal border of take-off platform and the target to determine the circular approach area around the target. In WT 1, we used a value of 117 pixels (3.2 cm) for the radius and in WT 2 a value of 71 pixels (2.7 cm).

Quantifying flies' approach with the "maximized A-B difference threshold"

To make the quantification of flies' approach behavior less arbitrary and to account for the fact that flies distributed differently in the two different wind tunnels and experimental sets, we calculated an approach area that segregated flies' approach probabilities for the attractive odorant A (or CS+) and the aversive odorant B (or CS-) the most. To determine the radius of this area, we took the Euclidean distance to target for each fly that was exposed to the attractive odorant A (or CS+) alone or the aversive odorant B (or CS-) alone; those flies that encountered mixtures of odorants were not incorporated in this process. The minimum distances were arranged in ascending order, and at each distance, we counted the number of flies from treatment A and treatment B that were included within this threshold distance. Thus for each of these distances, we calculated the difference in approach probabilities by:

Difference in approach probabilities = $\frac{A_{in}}{A_{in}+A_{out}} - \frac{B_{in}}{B_{in}+B_{out}}$

Where A_{in} represents the number of flies that were presented with odorant A and were included below the threshold, A_{out} is the number of flies presented with A but excluded above the threshold. B_{in} and B_{out} were the same measures for the flies that were presented with odorant B. We then plotted the thresholding index against the vector of minimum distances, and fitted a curve using locally weighted scatterplot smoothing using the R function "geom_smooth" with default parameters from the package "ggplot2", as this method avoids deviant points at further away regions in the scatterplot from affecting the local fit, and it highlights trends in data that may be unclear with a parametric fitting (Figure 3C and S1D, S1E, S2B, S2C, S3B and S3C). We took the distance that corresponded to the maximum peak of the curve as the radius of the approach area, as this point indicates the greatest separation between the two treatment groups. Since we used treatments A and B in defining the approach areas, we did not include these flies in the statistical analyses and restrict the comparisons to the mixtures.

Approach probability

In both WT 1 and WT 2 we filmed two angles of the flight area. Thus in each wind tunnel, there were two separate areas of approach, one for each of the two cameras for WT 1, and one for each side of the video screen for WT 2 (mirrored and original view). To calculate the approach probability, we gave each fly a binary score. The coordinate of each fly in every frame was recorded and tested as to whether it fell within the approach area boundaries. If a fly entered the approach area at any frame within 10 seconds after take-off, the fly was given a score of 1; if not, was given a score of 0. This was done for each camera (WT 1) or video side (WT 2), and then the results were combined so that only if a fly was in both areas of approach at the same time point, would it be given a score of 1. Finally, we calculated the proportion of flies in each treatment that entered the approach area to get the approach probability.

Visit probability maps

We extracted the x-y coordinates of the fly during the first ten seconds of flight. We divided the recording image into 20 x 20 pixel bins to create two visit probability maps. Each bin was represented by a cell in the map. We then plotted each coordinate point onto the visit map, giving the cell a score of 1 if one or more points fell into the bin, or a 0 if no points fell into the bin. For the flies that did not fly, a matrix of zeros was generated, with a score of 1 for the cell that represented the closest point on the take-off platform to the odor source. We calculated the mean for each pixel bin across all of the flies in a treatment group.

Response latency

We selected the flies that started flying within 10 000 frames after entering the take-off platform (111 s, corresponding to approximately 50 odorant pulses). We defined the individual response latency for each fly as the time point of flight minus the time point of entry onto the take-off platform.

Statistical Analysis

For all data analysis, R version 3.5.0 was used (R Core Team, 2012). All statistics were performed using Bayesian data analysis, based on (Korner-Nievergelt et al., 2015).

To investigate the effect of the synchronous and asynchronous mixtures on approach probability, we used a binomial generalized linear model (GLM), with approach probability as the binary response variable (1 = approach, 0 = no approach). We used the logistic regression (logit) link function. The synchronous and asynchronous mixtures were used as explanatory variables. We used an improper prior distribution (flat prior) and simulated 100 000 values from the posterior distribution of the model parameters using the function "sim" from the package "arm". The means of the simulated values from the posterior distributions of the model parameters were used as estimates, and the 2.5 % and 97.5 % quantiles as the lower and upper limits of the 95 % credible intervals. To test for differences between approach probabilities for the asynchronous and synchronous mixtures, we calculated the proportion of simulated values from the posterior distribution that were larger for asynchronous than for synchronous mixtures. We declared an effect to be significant if the proportion was greater than 0.95.

In the figures, we used different letters for comparisons between all stimuli and we used stars for comparisons between the synchronous mixture AB and the asynchronous mixtures. Posterior probabilities above 0.95 were indicated by "*" and above 0.99 by "**". A posterior probability of, for example, 0.96 for the comparison between the asynchronous mixture B33A and the synchronous mixture AB ($p(B33A > AB) = 0.96$) means that one can be 96% certain that flies' approach probability is greater for B33A than for AB.

To compare the response latencies across treatment groups, we modeled the response latency to the mixtures using a linear model with the synchronous mixture AB as the reference level. As in the previous model, the synchronous and asynchronous mixtures were used as categorical explanatory variables. Note that in this model we compared all combinations of mixtures within an experiment. We used the same methodology as before to simulate values from the posterior distribution and generate the means and the 95 % credible intervals. To test for differences, we calculated the proportion of draws from the posterior distribution for which the mean of each draw was smaller in one mixture than the mean of each draw of another mixture. We declared an effect to be significant if the proportion was greater than 0.95. If the posterior probability was higher than 0.95, it was deemed significantly different (with letters).

We also analyzed the behavioral data using frequentist statistics (Table S2). To see whether the asynchronous mixtures induced a significantly different approach probability than the synchronous mixture, we used an exact binomial test, using the R function "binom.test" from the R package "stats". We did the same comparisons as with the Bayesian analysis. For the experiment comparing BN, BA and blank air, we used the mean approach probability to BN (A) as the hypothesized probability of success. For each experiment involving synchronous mixtures, we used the mean approach probability to the synchronous mixture as the hypothesized probability of success. To compensate for multiple comparisons, we applied a Bonferroni correction by dividing the alpha level (0.05) by the number of comparisons within each experiment. We determined the result to be significant if the p value was smaller than the corrected alpha level.

SUPPLEMENTAL REFERENCES

Korner-Nievergelt, F., Roth, T., von Felten, S., Guélat, J., Almasi, B., Korner-Nievergelt, P., 2015. Bayesian data analysis in ecology using linear models with R, BUGS, and Stan. Academic Press.

R Core Team, 2012. R: A Language and Environment for Statistical Computing. R Foundation for Statistical Computing. R Found. Stat. Comput. Vienna, Austria.